Exploitation of surface acoustic waves to drive size-dependent microparticle concentration within a droplet†

Priscilla R. Rogers, James R. Friend and Leslie Y. Yeo*

Received 31st March 2010, Accepted 15th June 2010
DOI: 10.1039/c004822d

Ultrafast particle and cell concentration is essential to the success of subsequent analytical procedures and the development of miniaturized biological and chemical sensors. Here, surface acoustic wave (SAW) devices were used to excite a MHz-order acoustic wave that propagates into a microlitre droplet to drive spatial concentration and separation of two different sized suspended microparticles. The rapid concentration process, occurring within just three seconds to facilitate spatial partitioning between the two particle species, exploited two acoustic phenomena acting on the suspended particles: the drag force arising from acoustic streaming and the acoustic radiation force, both driving particles in different directions. This study elucidates the very intricate and interesting interplay of physics between fluid drag and acoustic forcing on the particles within a droplet, and, for the first time, demonstrates the existence of a frequency-dependent *crossover particle size* that can be used to effect species partitioning: depending on the operating frequency of the SAW device and the particle size, it is possible to cause one phenomenon to dominate over the other. A theoretical analysis revealed the extent to which each force would affect the particle trajectory (particle size range: 2–31 μm), subsequently verified through experimentation. Based on these findings, 6 and 31 μm polystyrene particles were successfully partitioned in a water droplet using a 20 MHz SAW device. This study reveals the suitability of using acoustic actuation methods for the useful partitioning of particle species within a discrete fluid volume.

1 Introduction

Microfluidic devices are proving superior to their well established, macroscale counterparts for conducting standard laboratory procedures. Lab-on-a-chip (LOC) devices, which employ microfluidic manipulation techniques, aspire to decrease sample consumption, shorten reaction times, lower analysis costs and increase portability with reduced footprints,[1] making them aptly suitable for point-of-care diagnostics and environmental sensors. On-chip particle and cell manipulation techniques play an important role in the development of such devices. One such need for particle manipulation is to overcome the typically low analyte concentration within a sample, which leads to detection sensitivity issues in the absence of preconcentration steps. For example, some bacterial strains require days of culturing in order to increase the count to a suitable level for detection. Using an ionic wind to generate a discharge driven vortex, Hou *et al.* showed that concentrating the bacteria to one location within a discrete microfluidic sample allowed for the successful detection of low-count bacteria samples.[2] Another need for particle manipulation arises from the fact that biological and chemical diagnostic procedures often require complete partitioning of the analyte from the many constituents found in complex physiological fluids, such as blood,[3] urine and saliva. This is to prevent the detection signals from other constituents interfering or masking the signal of the analyte. As such, rapid microparticle concentration and separation for preparative techniques are vital to the success of subsequent analytical procedures,[4] such as analyte detection.

Tsutsui and Ho[5] and Pamme *et al.*[6] provide comprehensive reviews on separation techniques currently employed in microfluidic systems. Common size-based separation techniques include filtration,[7,8] centrifugation[9,10] and hydrodynamic methods.[11–16] However, these techniques are often labor and time intensive, and are plagued with limitations such as complex geometries, high shear rates causing cell lysis, membrane pore size, filter fouling, moving parts, and/or difficulties in integration with downstream analytical processes. Other separation techniques include the use of electric fields,[17] magnetics,[18] and optics.[19] Whilst these techniques generally have high throughput cell separation and are not limited to size-based separation, these techniques often require powerful electric fields, magnetic tagging, or bulky laser optics.[5] The use of acoustics,[20,21] on the other hand, employ less invasive, non-contact manipulation for the separation of microparticles and cells.[22,23]

Miniaturized surface acoustic wave (SAW) devices, in which waves of nanoscale amplitude propagate along the free surface of a piezoelectric substrate, have proven to be ideal for lab-on-a-chip applications.[24] Unlike bulk acoustic waves (BAWs), in which propagation is not limited to the surface of the medium, SAWs exhibit lower acoustic energy losses and power consumption, and, as such, are highly suitable for microfluidic actuation. By driving fast acoustic streaming, with flow velocities on the order of mm/s to cm/s, SAW devices have been successfully utilized for droplet translation,[25] atomization,[26] mixing[27]

Micro/Nanophysics Research Laboratory, Department of Mechanical & Aerospace Engineering, Monash University, Clayton, VIC, 3800, Australia. E-mail: leslie.yeo@eng.monash.edu.au

† Electronic supplementary information (ESI) available: Additional data. See DOI: 10.1039/c004822d

and rapid particle concentration.[28,29] More recently, SAW devices exploiting acoustic radiation forces have also been utilized to align and separate two particle types within a microchannel using standing waves.[30,31]

The goal of this research is to employ SAWs to simultaneously concentrate and partition two different microparticle species within a discrete microfluidic volume. This simple approach removes the need for larger volumes of fluids and complex fabrication of channel geometries. This paper reports the novel coupling of the acoustic radiation force and the drag force (arising from acoustic streaming) acting on a particle suspension to drive size-dependent spatial concentration and partitioning in a sessile droplet atop the substrate of a SAW device. A theoretical estimate of these forces reveals the ability to drive the concentration phenomena with particle size and frequency as the only variables. These predictions are subsequently verified through experimental observations, following which the concentration and partitioning of particles of two different sizes is demonstrated. This research shows great promise for diagnostic LOC devices and is a positive step towards the detection of low concentration analytes in complex fluid samples.

2 Theory

For a sessile liquid droplet placed upon the substrate of a SAW device, strong absorption of incident SAW radiation occurs, whereby a longitudinal sound wave propagates into the droplet at the Rayleigh angle, θ_R.[32] Furthermore, for a droplet subject to asymmetric SAW distribution, bulk acoustic streaming is generated due to the closed volume of the droplet;[28] see Fig. 1(a). Raghavan *et al.*[29] described this three dimensional flow field in combination with Batchelor flows, which cause the particles to convect along streamlines under the influence of drag to the lower portion of the droplet *via* a helical trajectory, where they collect at the stagnation point in the centre of the droplet.

Specifically, acoustic streaming is the time-averaged steady flow that is forced by the action of Reynolds stresses, where the gradient in momentum flux that forces fluid to flow is associated with the dissipation of acoustic energy flux.[33,34] A suspended particle subjected to this streaming experiences a steady drag force. For microfluidic devices, in which the Reynolds number is typically of order one or less, the appropriate drag force on a spherical particle of radius R due to fluid flow is given by

$$F_D = 6\pi\mu UR \tag{1}$$

where U and μ is the relative streaming velocity and the dynamic viscosity of the fluid, respectively.

Depending upon factors such as the sound field frequency and particle size, the acoustic radiation force, *i.e.*, the net force attributed to the radiation pressure acting upon a particle's surface, can also be exploited for particle manipulation. Neglecting compressibility and viscous effects, the radiation force acting on a suspended solid sphere in an ideal fluid was first derived by King.[35] For a progressive sound wave, and when $|\dot{\xi}| = \kappa|A|$, where $|\dot{\xi}|$ is the fluid particle velocity, $|A|$ is the velocity potential, and κ is the wave number, the acoustic radiation force reduces to

$$F_{AR,L} = 2\pi\rho\left(\frac{2\pi f}{c_f}\right)^4 R^6 |\dot{\xi}|^2 \frac{1+\frac{2}{9}\left(1-\frac{\rho}{\rho_p}\right)^2}{\left(2+\frac{\rho}{\rho_p}\right)^2} \tag{2}$$

for $\kappa R \ll 1$. Here, ρ is the fluid density, ρ_p is the particle density, f is the frequency of the incident sound field and c_f is the sound

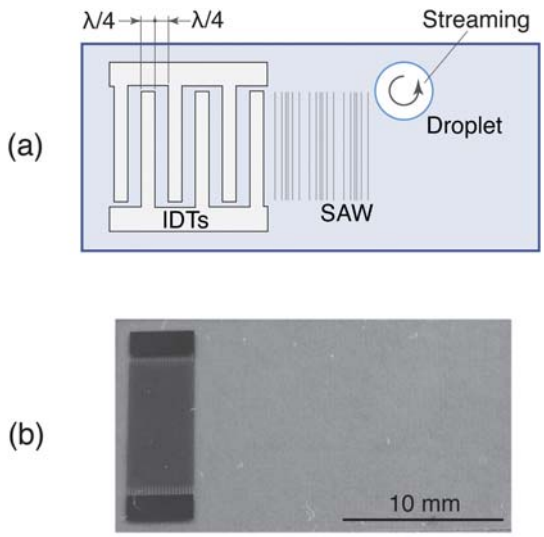

Fig. 1 (a) The propagating SAW wavelength λ is defined by the IDT finger width and spacing, both of which are $\lambda/4$. For a droplet subject to asymmetric SAW distribution, fast acoustic streaming is generated. The arrow represents the horizontal–plane projection of the acoustic streaming. (b) The SAW devices used in this study comprised a $LiNbO_3$ substrate with interdigital transducers (IDTs) patterned onto the substrate *via* standard fabrication techniques documented by Tan *et al.*[25] Note that the schematics drawn are not to scale.

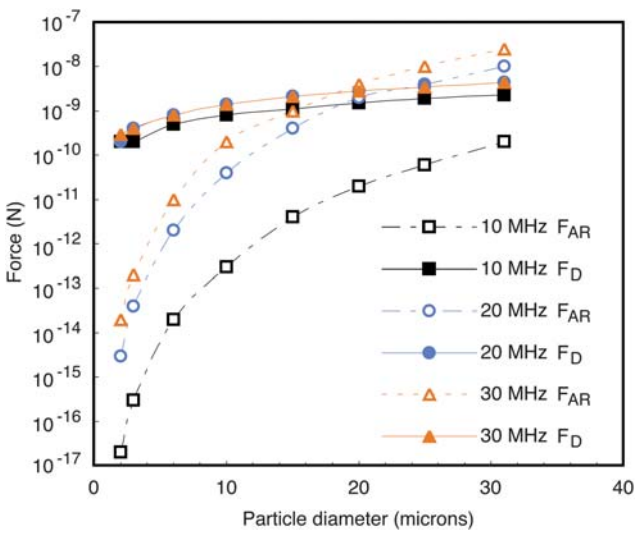

Fig. 2 Relative contribution and magnitude of the acoustic radiation force F_{AR} and the drag force F_D acting on the particle as a function of particle size and frequency. For the 10 MHz device (square data points), an equal magnitude and crossover is not achieved in this size range, resulting in the domination of Stokes drag on the behaviour of the particle. For the 20 MHz (circular data points) and 30 MHz (triangular data points) devices, the critical size range is between 20 and 25 μm, and 15 and 20 μm, respectively.

speed in the fluid medium. For larger particles, $\kappa R \geq 1$, higher order terms $O((\kappa R)^8)$ must be included.[35]

3 Theoretical analysis

Using eqn (1) and 2, the acoustically induced forces were estimated for polystyrene particles ($\rho_p = 1050$ kg/m^3) with diameters ranging from 2 to 31 μm suspended in water ($c_f = 1480$ m/s, $\rho = 1000$ kg/m^3) and subject to SAW sound field frequencies of 10, 20 and 30 MHz (see Section 4). The fluid particle velocity amplitude was assumed to be of the same order of magnitude as the SAW velocity amplitude on the piezoelectric substrate, which was experimentally measured using a laser Doppler vibrometer (MSA-400, Polytec Inc., Germany) as approximately 0.1, 0.3, and 0.3 m/s, for the 10, 20 and 30 MHz devices, respectively. Average fluid streaming velocities within the power range necessary to drive particle concentration (150–600 mW) were estimated within microlitre droplet volumes (1.5–3 μL) using commercially available 2D particle tracking software (Diatrack 3.01, Semasopht, Switzerland). Average values of 8, 15 and 15 mm/s were estimated for the 10, 20 and 30 MHz devices, respectively. The corresponding forces are given in Fig. 2.

In a comparative force analysis, the estimations shown in Fig. 2 highlight the rapid increase in radiation force with increasing particle size and frequency attributed to the R^6 and f^4 scaling in eqn (2), respectively. Generally, the acoustic radiation force is negligible for smaller particle sizes, yet becomes comparable in magnitude to, if not greater than, the drag force at larger particle sizes depending on the operating frequency of the SAW device. The size range over which the radiation force is of equal magnitude to the drag force is defined as the critical size range. Within this range, both the radiation force and drag force will contribute equally to the particle behaviour when subject to the ultrasound. Below this size range, however, the drag force due to acoustic streaming will dominate, and above this range, the acoustic radiation force dominates. For the particle sizes examined, the critical size range was not realized with the 10 MHz device. However, for the 20 MHz device, the range was between the 20 and 25 μm particle sizes, and between 15 and 20 μm for the 30 MHz device. This force comparison shows that

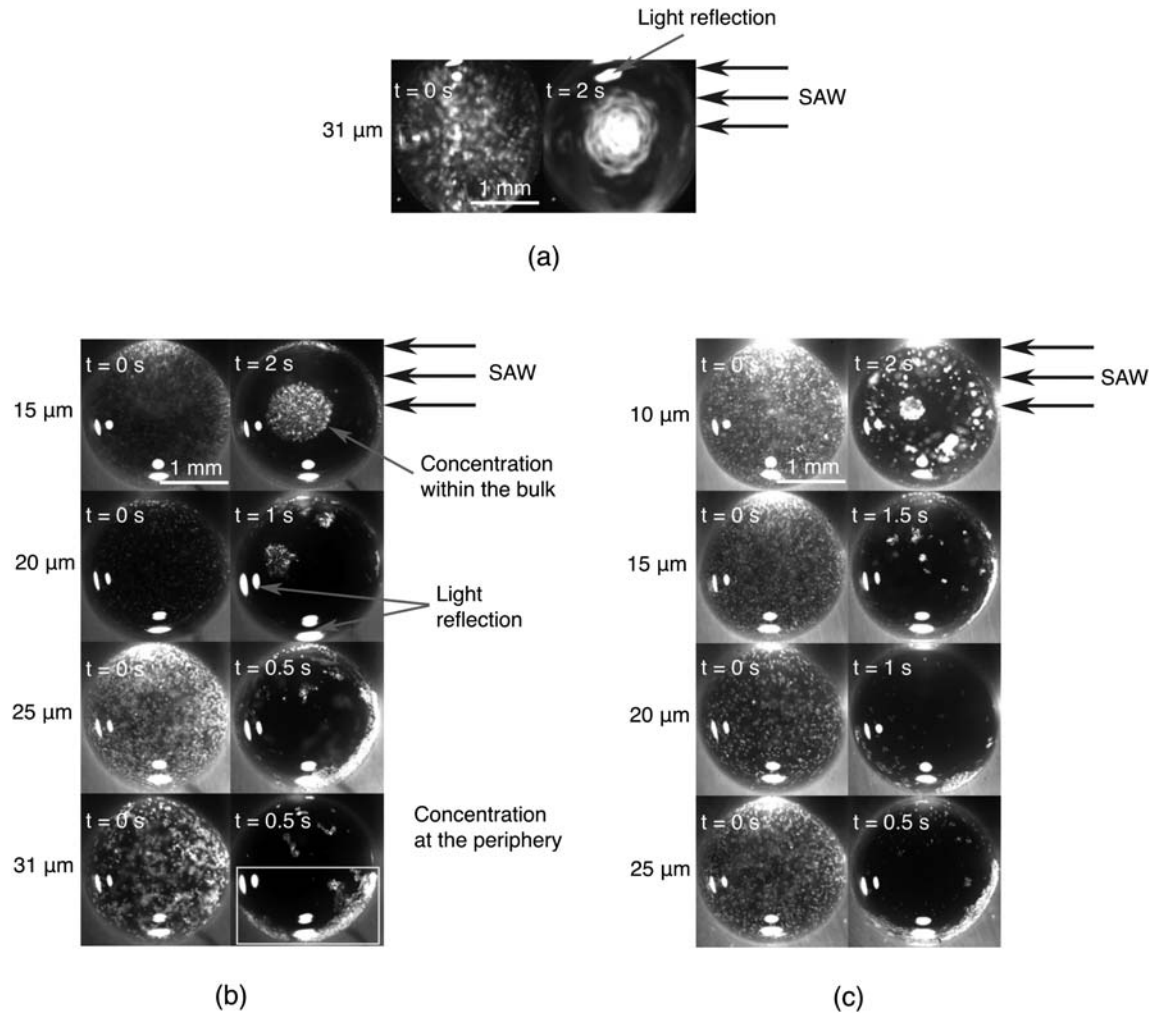

Fig. 3 (a) 31 μm particles placed upon a 10 MHz device are observed concentrate under the influence of drag. (b) The radiation force, on the other hand, plays an increasingly larger role on particle behaviour for the 20 MHz device, with most particles convected to the periphery of the droplet for 31 μm particles. Mixed behaviour is observed between the critical size range (20–25 μm). (c) The radiation force plays an even larger role with the 30 MHz device, and begins to affect the particle behaviour slightly before the critical size range (15–20 μm) is reached for 10 μm particles.

it is possible to manipulate particle behaviour based on both SAW frequency and particle size.

4 Experiments

The three SAW devices used in this study consisted of 0.5 mm thick, 128° rotated Y–cut, X–propagating lithium niobate substrate ($LiNbO_3$, Roditi, United Kingdom); see Fig. 1(b). The dual layer (Al/Cr) interdigital transducers (IDTs) comprised straight finger pairs (typically 20) and were actuated at their characteristic resonant frequency, *i.e.*, 10, 20 and 30 MHz. To facilitate accurate comparison between the theoretical analysis and experimentation, all parameters listed in the previous section were maintained during experimentation. The input power was supplied to the SAW device by a signal generator (Rhode & Schwarz SML 01, Germany) and amplifier (Amplifier Research 10W1000C, USA), and measured using a digital oscilloscope (Tektronix TDS3014B, USA). Polystyrene microspheres (Thermo Scientific and Bioscientific, Australia) were suspended in deionised water at individual concentrations on the order of 10^6 particles/mL. For particle partitioning, 6 and 31 μm particles and a 20 MHz SAW device were used as these two different particle sizes straddled the crossover particle size range (20–25 μm) determined in Section 3. The microlitre droplet was viewed using a stereomicroscope (Olympus BXFM, Japan) coupled to a high speed video camera (Olympus iSpeed, Japan, for colour images, and Mikotron, Germany, for monochromatic images), for which illumination was supplied by a mercury light source (EXFO X-Cite 120) and a proprietary 120 W short arc lamp (Olympus, Japan). Based on the partitioning results obtained, the 6 μm particle behaviour was deemed to require further analysis. The optimum power for the 6 μm particles was determined using a normalised pixel intensity analysis (NPI),[28] where the concentration time was defined as the time at which the NPI was no longer changing, *i.e.*, the time beyond which no further particle aggregation occurred.

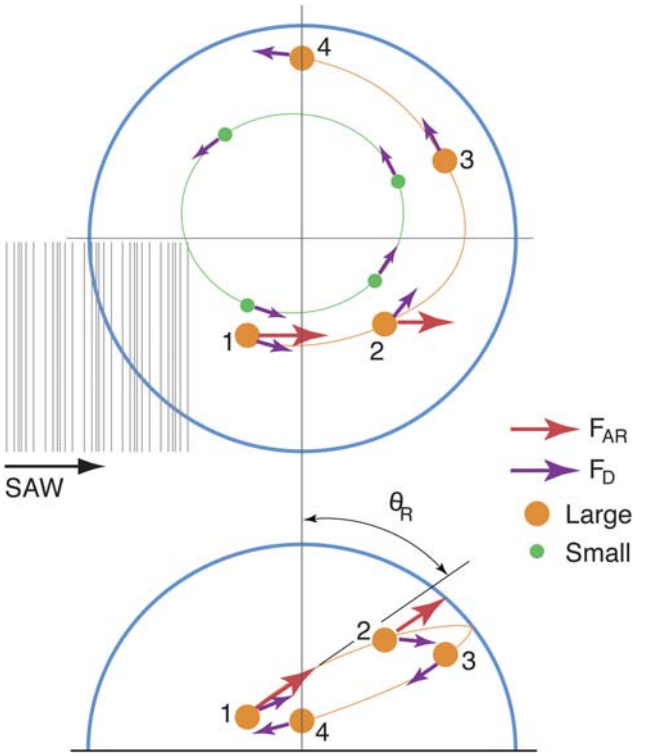

Fig. 4 Larger particles (the size of which are frequency dependent) are dominated by radiation force with the drag force playing a smaller role on the overall particle trajectory. The larger particles in position 1 are driven toward the free surface of the droplet. The effect of acoustic streaming at positions 1–4, however, causes the particles to circulate within a portion of the droplet before they reach the periphery near position 4. The smaller particles recirculate within the droplet until they concentrate in the centre under the influence of drag. The side view for the smaller particles is omitted for simplicity. For visualisation purposes, the SAW enters from the bottom left corner as opposed to the top right corner in Fig. 3.

5 Results and discussion

The increased dominance of the radiation force with increasing particle size for each SAW operating frequency can be observed in Fig. 3. Generally, two distinct particle responses are evident. The first involved the concentration of the particles in the centre of the droplet resulting from the dominance of the drag force arising from acoustic streaming, as reported by Raghavan *et al.*[29] The second involved particle aggregation at the periphery of the droplet on the side opposite to the incident SAW, indicating the dominance of radiation force. This new observation can be explained by considering the force magnitudes and directions acting on a particle at different stages in the droplet (Fig. 4). As the longitudinal sound wave is induced into the droplet at the Rayleigh angle, the radiation force acts to drive the particles toward the free surface of the droplet along this line of action. However, with the combined effect of the weaker drag force, the particles recirculate within a portion of the droplet under the influence of drag, whilst being forced toward the free surface of the droplet where the acoustic radiation is at a minimum. Between these two distinct responses, especially within the critical size range, the particles are neither entirely concentrated in the centre of the droplet nor entirely convected to the periphery.

Closer inspection of Fig. 3 reveals that the experimental results support the theoretical analysis, indicating a valid approximation for an order of magnitude analysis using King's formula.[35] As determined in Section 3 for the 10 MHz device, the radiation force does not contribute to particle motion for the size range examined; even the largest particle size, *i.e.*, the 31 μm particles, is observed to concentrate in the centre of the droplet (Fig. 3(a)). For the 20 and 30 MHz devices, either force plays a dominant role depending upon the particle size. For the 20 MHz device (Fig. 3(b)), the radiation force begins to oppose particle concentration within the centre of the droplet for particles of sizes 20 μm or larger. This supports the theoretical analysis in Section 3, which predicts the radiation force to be of an equal order of magnitude to the drag force for particle sizes between 20 and 25 μm. Above this critical size range, the particles were driven to the periphery under the influence of the dominant radiation force, aside from a small number of particles that had already sedimented and adhered to the substrate surface before

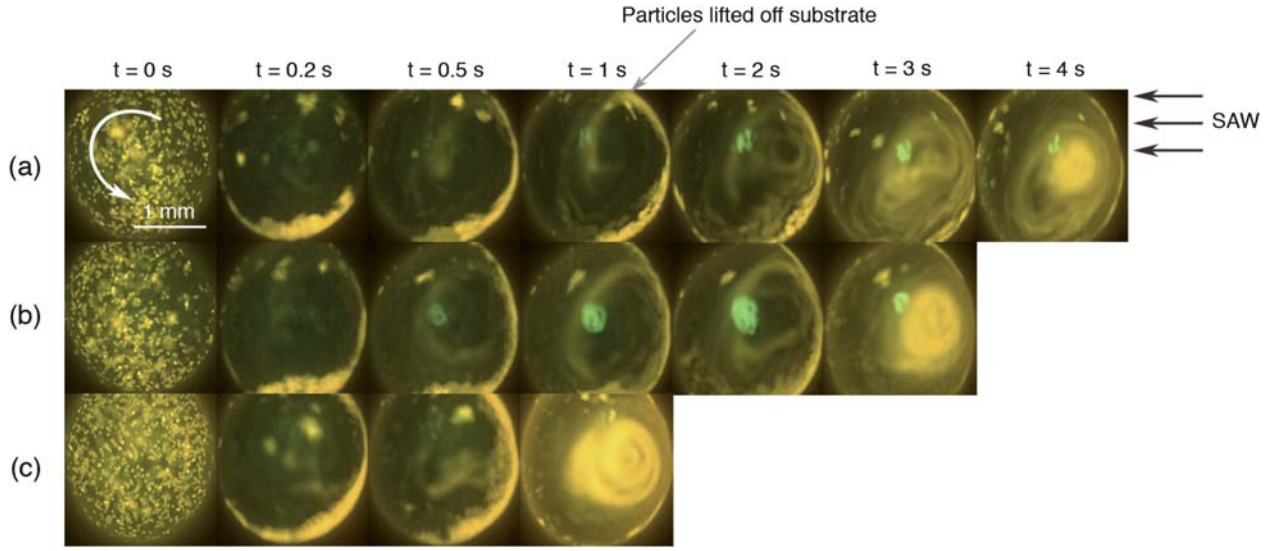

Fig. 5 (Colour online) Concentration and partitioning of 6 μm (green) and 31 μm (yellow) particles at input powers of (a) 250 mW, (b) 420 mW and (c) 600 mW, respectively. The 6 μm particles concentrate within the bulk of the droplet, whilst the 31 μm particles are driven to the periphery of the droplet, and subsequently concentrated on the free surface of the droplet. The droplet rotation direction is indicated by the arrow.

the power was turned on. Experiments conducted using the 30 MHz device (Fig. 3(c)) also support the theoretical analysis, with a critical size range of 15–20 μm. The only deviation from the theoretical analysis is that the radiation force plays a greater role on the 10 μm particles than predicted.

Based on these initial experimental findings, 6 and 31 μm fluorescent particles were suspended in a single 1.5 μL droplet atop a 20 MHz device as these particle sizes straddled the critical size range (20–25 μm) determined in Section 3. Fig. 5 shows particle partitioning for a range of input powers. For all powers, the 6 μm particles (green fluorescing) are observed to begin concentration in the centre of the droplet almost immediately, whilst the 31 μm particles are driven to the periphery of the droplet, followed by subsequent concentration on the free surface at times beyond 1s. Interestingly, rather than the 31 μm particles remaining stationary at the periphery of the droplet, they were gradually dragged around the periphery under the influence of the drag force to the point of the SAW radiation incidence (Fig. 5). Once there, the particles were lifted off the substrate due to the dominant radiation force and began recirculating on the free surface of the droplet due to acoustic streaming. Subsequently, concentration of the 31 μm particles at the top of the droplet's free surface was observed as opposed to the concentration of the 6 μm particles within the bulk of the droplet (see figure in Electronic Supplementary Information†). This new observation indicates that another concentration mechanism, distinctly different from that of the bulk concentration mechanism described by Raghavan *et al.*,[29] is at play. During experimentation, it was noted that if there was a lower concentration of 31 μm particles suspended in the droplet than 10^6 particles/mL, concentration on the free surface became increasingly unlikely. Hence, given that shear-induced migration is dependent upon an initial localised close packing fraction along the fluid streamlines,[29] it is believed to be the underlying mechanism behind particle concentration on the free surface of the droplet.

From Fig. 5 it is evident that increasing the input power decreases the concentration time of the 31 μm particles from approximately 4 s at 250 mW (Fig. 5(a)) to 1 s at 600 mW (Fig. 5(c)). This can be attributed to the faster streaming velocities that are generated at higher powers.[27] As a consequence, the 31 μm particles experience a larger drag force at higher powers. This facilitates faster particle transport around the periphery of the droplet to the point where they are lifted off the substrate, after which concentration on the free surface commences. The 6 μm particles, however, do not follow such a simple trend. From Fig. 5, it can be seen that the most effective partitioning occurs at 420 mW (Fig. 5(b)), with smaller concentration spots at 0.5 s for powers of 250 and 600 mW (Fig. 5(a) and 5(c), respectively). As a result, at lower powers, the concentration of the 6 μm particles in the bulk is incomplete before the 31 μm particles begin to concentrate on the free surface. Similarly, at higher powers, where the 31 μm particles concentrate even faster, the 6 μm particles are unable to completely concentrate within the bulk.

Whilst partitioning is achieved upon driving the larger particles to the periphery of the droplet, the complete concentration

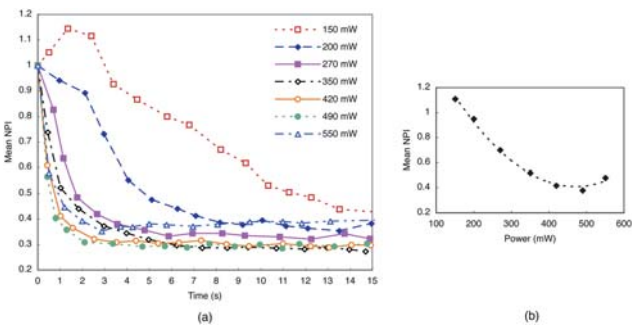

Fig. 6 (a) The drag induced concentration process of the 6 μm particles is a function of input power. Lines were added for visualization purposes. The concentration time is defined by the NPI reaching a constant. (b) The optimum power is observed to be between 400 and 500 mW.

of both particle sizes hinges upon the concentration process of the 6 μm particles. On this basis, we examined the concentration of the 6 μm particles in the absence of the 31 μm particles at various input powers. Fig. 6(a) shows the extent of the particle concentration as a function of time. We observed that maximum concentration, indicated by the lowest value of NPI obtained, occurs at an optimum power range of between 400 and 500 mW (Fig. 6(b)). This is consistent with Li *et al.*[28] who noted that above a threshold input power, the acoustic streaming is sufficiently strong to redisperse the particles, and hence oppose the particle concentration. Furthermore, at 420 mW, maximum concentration occurs within 3 s (Fig. 6(a)), consistent with the results in Fig. 5(b) where the 6 μm particles are observed to completely concentrate in the bulk before the 31 μm particles begin to concentrate on the free surface, yielding effective concentration and partitioning of both particle sizes.

These results illustrate the ease with which experimental parameters, such as the input power, can be adjusted to achieve a desired outcome, such as the detection of one or both concentrated species. For example, optical detection methods that use highly focused lasers, such as Raman spectroscopy, could easily traverse the droplet in order to detect either or both species. More specifically, in terms of the microfluidics, if detection of the smaller particles was desired, then the optimum concentration power of these particles would be supplied to the device. In this circumstance, the input power would be supplied to the device until the smaller particles were completely concentrated, at which point the larger particles would remain removed to the periphery of the droplet, where they would not interfere or mask the detection of the smaller particles. On the other hand, if detection of the larger particles was desired, then higher powers could be supplied to the droplet in order to induce their rapid concentration on the free surface. Finally, if detection of both particle types was preferred, then by supplying the optimum power of the smaller particles to the device, rapid detection of the smaller particles could take place first, followed by the detection of the larger particles at a later time. Alternatively, detection could take place from the side of the droplet once both particle types are fully concentrated.

As a proof–of–concept, this process can also be employed for the selective concentration and separation of biological species from non-biological particles. For example, the detection of low concentration airborne allergens, such as pollen, is necessary to predict whether susceptible patients are likely to experience allergic reactions. Often such a sample will also include airborne particulate matter, either naturally occurring, such as dust or sea spray, or man-made, such as those from industrial activities. Fig. 7 shows the concentration and partitioning of paper mulberry pollen (12–13 μm, Polysciences, Inc., Australia) from the 31 μm synthetic particles, which were selected to represent harmless particulate matter. Noting that the radiation force will be approximately two orders of magnitude lower than that predicted for polystyrene due to compressibility effects,[36] the pollen concentrates under the influence of drag, whilst the radiation force drives the synthetic particles to the periphery as in previous experiments. As the ultimate goal is to concentrate the pollen to a suitable level for detection, there is no requirement for the concentration of the synthetic particles. As such the power was switched off upon concentration of the pollen at 3 s.

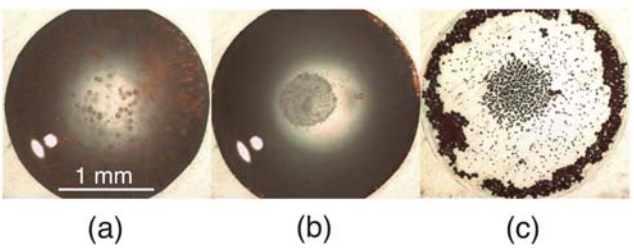

Fig. 7 Separation of the pollen and synthetic particles. (a) Initially, the pollen and synthetic particles were suspended homogeneously throughout the entire droplet. (b) After 3 s, the pollen particles concentrated in the centre of the droplet, and are hence separated from the synthetic particles, which concentrated along the periphery of the droplet. (c) The two species remain separated even after the droplet is fully evaporated after 1 min.

6 Conclusions

Using SAWs, this paper demonstrates a simplistic method for the concentration and partitioning of two different sized microparticle types within a discrete microfluidic volume. *Via* the careful selection of SAW frequency (MHz order), two acoustic forces, namely the radiation force and the drag force arising from acoustic streaming, were novelly coupled and exploited for particle manipulation. Generally, within the particle size range tested (2–31 μm), the drag force dominated for smaller particle sizes, whilst the radiation force became comparable, if not dominant, for larger particle sizes at frequencies above 10 MHz. Accordingly, these forces were exploited successfully for the concentration and partitioning of 6 and 31 μm particles in a microlitre droplet using a 20 MHz SAW device. The smaller particles first concentrated in the bulk of the droplet due to the dominant drag force, whilst the larger particles were driven to the periphery under the influence of the radiation force, and subsequently concentrated on the free surface of the droplet. These findings illustrate the possibility of using these two acoustic actuation methods for the ultrafast concentration and partitioning of cells and biomolecules in discrete fluid systems using microfluidic SAW devices, which is essential for diagnostic procedures such as analytical detection.

References

1 G. Whitesides, *Nature*, 2006, **442**, 368–373.
2 D. Hou, S. Maheshwari and H. Chang, *Biomicrofluidics*, 2007, **1**, 014106.
3 M. Toner and D. Irimia, *Annu. Rev. Biomed. Eng.*, 2005, **7**, 77–103.
4 F. Priego-Capote and M. de Castro, *J. Biochem. Biophys. Methods*, 2007, **70**, 299–310.
5 H. Tsutsui and C. Ho, *Mech. Res. Commun.*, 2009, **36**, 92–103.
6 N. Pamme, *Lab Chip*, 2007, **7**, 1644–1659.
7 V. VanDelinder and A. Groisman, *Anal. Chem.*, 2006, **78**, 3765–3771.
8 T. Crowley and V. Pizziconi, *Lab Chip*, 2005, **5**, 922–929.
9 M. Madou, J. Zoval, G. Jia, H. Kido, J. Kim and N. Kim, *Annu. Rev. Biomed. Eng.*, 2006, **8**, 601–628.
10 J. Seo, M. Lean and A. Kole, *Appl. Phys. Lett.*, 2007, **91**, 033901.
11 Y. Sai, M. Yamada, M. Yasuda and M. Seki, *J. Chromatogr., A*, 2006, **1127**, 214–220.
12 A. Bhagat, S. Kuntaegowdanahalli and I. Papautsky, *Phys. Fluids*, 2008, **20**, 101702.

13 L. Huang, E. Cox, R. Austin and J. Sturm, *Science*, 2004, **304**, 987–990.
14 J. Takagi, M. Yamada, M. Yasuda and M. Seki, *Lab Chip*, 2005, **5**, 778–784.
15 D. Yoon, J. Ha, Y. Bahk, T. Arakawa, S. Shoji and J. Go, *Lab Chip*, 2009, **9**, 87–90.
16 Z. Wu, B. Willing, J. Bjerketorp, J. Jansson and K. Hjort, *Lab Chip*, 2009, **9**, 1193–1199.
17 J. Voldman, *Annu. Rev. Biomed. Eng.*, 2006, **8**, 425–454.
18 N. Pamme, J. Eijkel and A. Manz, *J. Magn. Magn. Mater.*, 2006, **307**, 237–244.
19 K. Dholakia, P. Reece and M. Gu, *Chem. Soc. Rev.*, 2008, **37**, 42–55.
20 F. Petersson, L. Aberg, A. Sward-Nilsson and T. Laurell, *Anal. Chem.*, 2007, **79**, 5117–5123.
21 S. Kapishnikov, V. Kantsler and V. Steinberg, *Journal of Statistical Mechanics: Theory and Experiment*, 2006.
22 T. Laurell, F. Petersson and A. Nilson, *Chem. Soc. Rev.*, 2007, **36**, 492–506.
23 M. Wiklund and H. Hertz, *Lab Chip*, 2006, **6**, 1279–1292.
24 L. Yeo and J. Friend, *Biomicrofluidics*, 2009, **3**, 012002.
25 M. Tan, J. Friend and L. Yeo, *Lab Chip*, 2007, **7**, 618–625.
26 A. Qi, J. Friend, L. Yeo, D. Morton, M. McIntosh and L. Spiccia, *Lab Chip*, 2009, **9**, 2184–2193.
27 R. Shilton, M. Tan, L. Yeo and J. Friend, *J. Appl. Phys.*, 2008, **104**, 014910.
28 H. Li, J. Friend and L. Yeo, *Biomed. Microdevices*, 2007, **9**, 647–656.
29 R. Raghavan, J. Friend and L. Yeo, *Microfluid. Nanofluid.*, 2010, **8**, 73–84.
30 J. Shi, X. Mao, D. Ahmed, A. Colletti and T. J. Huang, *Lab Chip*, 2008, **8**, 221–223.
31 J. Shi, H. Huang, Z. Stratton, Y. Huang and T. J. Huang, *Lab Chip*, 2009, **9**, 3354–3359.
32 A. Wixforth, *Superlattices Microstruct.*, 2003, **33**, 389–396.
33 J. Lighthill, *J. Sound Vib.*, 1978, **61**, 391–418.
34 N. Riley, *Theor. Comput. Fluid Dyn.*, 1998, **10**, 349–356.
35 L. King, *Proc. R. Soc. London, Ser. A*, 1934, **147**, 212–240.
36 K. Yosioka and Y. Kawasima, *Acustica*, 1955, **5**, 167–173.